

COMPONENT PART NOTICE

THIS PAPER IS A COMPONENT PART OF THE FOLLOWING COMPILATION REPORT:

(TITLE): Proceedings of the Conference on Improvement of Aerodynamic Performance  
through Boundary Layer Control and High Lift Systems Held at the  
Fluid Dynamics Panel Symposium in Brussels, Belgium on 21 23 May 1984.

(SOURCE): Advisory Group for Aerospace Research and Development, Neuilly-sur-Seine  
(France).

TO ORDER THE COMPLETE COMPILATION REPORT USE AD A147 396.

THE COMPONENT PART IS PROVIDED HERE TO ALLOW USERS ACCESS TO INDIVIDUALLY AUTHORED SECTIONS OF PROCEEDINGS, ANNALS, SYMPOSIA, ETC. HOWEVER, THE COMPONENT SHOULD BE CONSIDERED WITHIN THE CONTEXT OF THE OVERALL COMPILATION REPORT AND NOT AS A STAND-ALONE TECHNICAL REPORT.

THE FOLLOWING COMPONENT PART NUMBERS COMPRISE THE COMPILATION REPORT:

- |      |          |        |   |
|------|----------|--------|---|
| AD#: | P004 052 | TITLE: | Recent Progress on Development and Understanding of High Lift Systems.  |
|      | P004 053 |        | Investigations into the Effects of Scale and Compressibility on Lift and Drag in the RAE 5m Pressurised Low-Speed Wind Tunnel.    |
|      | P004 054 |        | Recent Advances in Computational Methods to Solve the High-Lift Multi-Component Airfoil Problem.                                  |
|      | P004 055 |        | Inviscid Compressible Flow Past a Multi-Element Airfoil.  |
|      | P004 056 |        | Design of an Airfoil Leading Edge Slat Using an Inverse Aerodynamic Calculation Method.   |
|      | P004 057 |        | Modelling Circulation Control by Blowing.   |
|      | P004 058 |        | Turbulent Bubbles behind Airfoils and Wings at High Angle of Attack.  |
|      | P004 059 |        | Aerodynamic Issues in the Design of High-Lift Systems for Transport Aircraft.   |
|      | P004 060 |        | An Update of the Canada/U.S.A. Augmentor-Wing Project.  |
|      | P004 061 |        | Aircraft Drag Reduction Technology.   |
|      | P004 062 |        | Theoretical Study of Boundary-Layer Control.  |
|      | P004 063 |        | Drag Reduction due to Boundary-Layer Control by Combined Blowing and Suction.   |
|      | P004 064 |        | Design Studies of Thick Laminar-Flow Airfoils for Low Speed Flight Employing Turbulent Boundary Layer Suction over the Rear Part. |
|      | P004 065 |        | Technology Developments for Laminar Boundary Layer Control on Subsonic Transport Aircraft.  |
|      | P004 066 |        | Turbulent Drag Reduction Research.  |
|      | P004 067 |        | On the Relaxation of a Turbulent Boundary Layer after an Encounter with a Forward Facing Step.                                    |
|      | P004 068 |        | Full Scale Experiments into the Use of Large-Eddy Breakup Devices for Drag Reduction on Aircraft.                                 |

REPRODUCED AT GOVERNMENT EXPENSE

COMPONENT PART NOTICE (CON'T)

AD#: P004 069 TITLE: Pneumatic Turbulators - A Device for Drag  
Reduction at Reynolds Numbers below 5, 000, 000.  
P004 070 Active and Passive Shock/Boundary Layer  
Interaction Control on Supercritical Airfoils.  
P004 071 Transonic Shock Interaction with a Tangentially-  
Injected Turbulent Boundary Layer.

## AD-P004 057

## MODELLING CIRCULATION CONTROL BY BLOWING

M.M. Soliman, Research Fellow, Southampton University  
 R.V. Smith, Chief Project Engineer, Westland Helicopters, Yeovil  
 I.C. Choosman, Professor of Helicopter Engineering, Southampton University, UK.

## SUMMARY

This paper describes a new theoretical representation of circulation control based on discrete vortex modelling techniques. The application of discrete vortex modelling to the prediction of circulation control is initially presented for the Coanda flow of a wall jet around a circular cylinder in a free stream. The decay in the jet momentum, due to viscous and entrainment effects, has been represented in the model by decaying the strength of each vortex as it flows downstream from the slot. The model's application has then been extended to predict the effect of circulation control on other shapes of aerofoil. The paper includes the application of the model to an elliptic section as an example of any aerofoil section that can be represented in a potential flow. The model has had considerable success in predicting the lift produced from such bodies due to the jet, but information about the drag requires additional modelling of the surface boundary layer. A similar technique has been used to represent the boundary layer by discrete vortices and doublets. The model's prediction has been compared with the experimental data of an unblown circular cylinder.

$C$	: Chord
$C_L$	: Lift coefficient
$C_D$	: Drag coefficient
$C_J$	: Jet momentum coefficient
$d$	: Vortex distance
$K$	: Arbitrary decay constant
$q$	: Tangential velocity
$R_0$	: Radius of the cylinder
$r_v$	: Radial position of a vortex
$r_i$	: Radial position of an image vortex
$R_b$	: Radial distance of the outer edge of boundary layer
$R_d$	: Radial distance of the outer edge of displacement thickness
$t$	: Age of a vortex
$t_j$	: Slot thickness
$U_\infty$	: Free stream velocity
$\gamma$	: Vortex strength
$\gamma_0$	: Initial vortex strength
$\delta_d$	: Displacement thickness

## 1. INTRODUCTION

The concept of circulation control for high lift generation was developed in the early 1960's at the National Gas Turbine Establishment and has since been investigated by a number of researchers. Early work in the subject had investigated the lift and drag characteristics of two-dimensional circular and elliptic cross-sections with circulation control (References 1-4). Later work extended the application of circulation control concept to helicopter rotors (References 5-6). The main current research effort is the X-wing, being developed for the US Navy and DARPA (References 7-9).

Circulation control relies for lift generation on the ability of a wall jet to control the separation point at the bluff trailing edge of an aerofoil. Conventional aerofoils feature a sharp trailing edge which effectively determines the location of the rear stagnation point. The rear stagnation point of an aerofoil with a non-sharp trailing edge is not constrained in this manner, and its location can be controlled by a wall jet. Control of the aerofoil circulation results in, what is known as, "circulation control by blowing".

The relationship between the lift generated by a circulation control aerofoil and the wall jet momentum supplied reflects a complex interaction of the aerofoil design parameters. Factors influencing performance include the aerofoil shape, leading and trailing edge design, blowing slot width and the number of slots as well as slot(s) position. The performance of an arbitrary circulation control aerofoil is determined by the interaction of these design parameters. If a theoretical model does not correctly represent the effects of these parameters, it will fail to model an arbitrary circulation control aerofoil. The lack of a generalized performance prediction method has restricted circulation control development and applications despite its promising performance.

## 2.1 CONVENTIONAL CIRCULATION CONTROL MODELLING

There have been several efforts to predict the performance of an arbitrary circulation control aerofoil, all based on a conventional boundary layer approach to the problem. This approach was developed initially by Dunham (Reference 10) to predict the flow about a circular cylinder fitted with a wall jet exhausting near tangentially to its surface. Dunham's method relied on the conventional boundary layer and wall jet calculations to decide the pressures at the separation points on the upper and lower surfaces. A solution was reached when a certain jet strength satisfied Thwaites condition (Reference 11) of equal separation pressures at the upper and lower surfaces.

The model's accuracy of prediction depended on the assumptions made regarding the wall jet representation, flow entrainment from the outer flow to the jet, and the separation criterion. Dunham's model satisfactorily predicted circulation control performance trends at low momentum coefficients (Figure 1). However, the numerical accuracy became poor at high momentum coefficients with small slot widths or when analysing single slot models. This accuracy reflected the sensitivity of the model to the treatment of separation and entrainment. These became significant considerations when the length of the surface between the blowing slot(s) and the separation point was large, either at high momentum coefficient, or when only one slot was employed at a position far from the separation point.

Similar methods have been developed (References 12-13), but all these methods relied on successful development of semi-empirical expressions to treat turbulent boundary layers and wall jets over curved surfaces in the presence of an arbitrary pressure gradient. Although encouraging results have been obtained using this technique, a more fundamental approach is desirable. It is desirable that such an approach should be sufficiently general to allow treatment of the many applications of boundary layer control and Coanda flows in contemporary aerodynamics. A new model is developed, and described below, which is based on a discrete-vortex approximation to the shear layer external to a wall jet under an external stream.

## 2.2 DISCRETE VORTEX MODELLING OF CIRCULATION CONTROL

Discrete-vortex modelling consists of the representation of a shear layer, by a number of discrete vortex filaments surrounded by an inviscid, irrotational flow. Deformation of the sheet is calculated by evaluating the velocity induced at each element by the remaining elements and satisfying the boundary conditions of the initial flow. Discrete-vortex modelling has been applied to a wide range of flows which include shear layer(s). Rosenhead (Reference 14) applied this technique to the shear layer formed between two uniform streams of flow with equal speed in opposite directions. The same technique was used to represent the two shear layers separating a stream from an exterior stream flowing with equal speed in the opposite direction (Reference 15). Gerrard (Reference 16) adapted this approach to model the wake shed by a bluff body, the shear layer at the wake boundary being represented by discrete vortices introduced into the flow at successive time steps.

The application of this technique to circulation control was developed initially for circular cylinders (Reference 17), then extended later for other forms of aerofoils (Reference 18). Several modifications and developments have been introduced since, and the latest form of the models is presented below.

### 3.1 MODEL DESCRIPTION

Initially, the flow about a circular cross-section in a uniform stream is modelled with zero circulation. The circular boundary is formed by introducing a doublet into the uniform stream. The shear layer formed at the edge of the jet is represented by a series of discrete vortices. The shear layer is formed as the jet emerges from the slot, so the vortices are introduced progressively to simulate the growth of the jet as it leaves the slot and flows downstream. The first vortex is introduced at a point above the circular boundary where the slot is located. The distance of this point from the boundary is the slot width. The vortex is accompanied by an image vortex inside the boundary, with the same strength but opposite sense of rotation. The position of the image vortex is decided by the equation:

$$R_v R_i = R_0^2 \quad (1)$$

where  $R_v$  : Radial distance of the vortex  
 $R_i$  : Radial distance of the image vortex  
 $R_0$  : Radius of the circular boundary

The reason for introducing the image vortex is to preserve the shape of the circular boundary by ensuring the absence of any normal velocity at the circular boundary. The external vortex moves a specified distance step after calculating the induced velocities on this vortex by all elements of the flow field, including its image. The image vortex position is readjusted according to equation (1), while a new vortex is introduced at the slot lip with its image. The process is repeated, allowing each vortex to move a distance proportional to the time taken by the initial vortex to move over the fixed distance-step, and also to the local velocity of the vortex in question. After each step, a new vortex/image is introduced at the slot lip. The process leads eventually to a sheet of discrete vortices as shown in Fig.2.

### 3.2 JET DECAY

In the real flow, the jet momentum decays due to viscous and mass entrainment effects. As a segment of the jet mass flow leaves the slot and flows downstream, a gradual loss of its momentum occurs due to viscosity and entrainment from the external flow. This loss in momentum may be represented in the model by the use of a time dependent vortex decay. The rate of loss of momentum is expected to be in proportion to the initial jet momentum and the external flow momentum. Therefore, an arbitrary form of decay has been adopted in the model by reducing the vortex strength as it flows from the slot. Assuming that the initial strength of the vortex is  $\gamma_0$ , then its strength will be reduced to the value

$$\gamma(t) = \gamma_0 \cdot \text{EXP}(-K U_\infty \gamma_0 t / d) \quad (2)$$

where  $U_\infty$  : Free stream velocity  
 $d$  : Distance step  
 $t$  : Time age of the vortex  
 $K$  : Arbitrary constant

The value  $(\gamma_0/d)$  represents the circulation per unit length of the shear layer when the jet leaves the slot, hence it can be used as a measure of the jet momentum. The value  $U_\infty$  is a measure of the momentum of the external flow. The chosen form of decay obeys the observed conditions that the strength of the vortex becomes zero as its age increases indefinitely and that its decay is most rapid, when the vortex age is small and the shear is greatest.

### 3.3 CALCULATION OF THE LIFT AND JET MOMENTUM COEFFICIENTS ( $C_L$ and $C_J$ )

The lift coefficient ( $C_L$ ) is calculated by integrating the normal local pressure coefficients ( $C_{p\lambda}$ ) on the circular boundary, determined as usual from

$$C_{p\lambda} = 1 - (U_\lambda/U_\infty)^2$$

where  $U_\lambda$  = local velocity induced by all the flow elements.

The jet mass flow rate ( $\dot{m}$ ) is defined as  $\rho V_j t_j$ , where  $V_j$  is the mean jet velocity at the slot exit,  $t_j$  is the jet thickness at the slot.  $V_j$  is calculated in the model as the surface velocity beneath the slot lip and defined as  $V_s$ . The jet momentum is then defined as the product of  $\dot{m}$  and the increment in surface velocity beneath the slot ( $\Delta V$ ) due to the presence of the jet. In defining this jet momentum, a primary consideration is that the momentum coefficient predicted should be zero when no air is supplied to the blowing system. Therefore the jet momentum coefficient is calculated as:

$$C_J = (V_s \Delta V t_j) / (U_\infty^2 R_0)$$

where  $V_s$  is the total surface velocity at the slot and  $\Delta V$  is the velocity induced at the surface by the vortices only.

### 4.1 MODEL CONVERGENCE AND SENSITIVITY TO VORTEX SPACING

The lift and momentum coefficients will be reliably predicted when the following conditions are met:-

- 1) the geometry of the jet sheet should stabilise so that the introduction of additional vortices have no effect on it
- 2) the vortex spacing used to model the jet sheet should not affect the lift and momentum coefficients.

In the previous sections it has been shown that the process of introducing vortices at the slot lip eventually led to a fixed geometry for the jet sheet which was unaffected by the introduction of further vortices at the slot lip, thus satisfying condition (1) above.

Condition 2 was tested by evaluating  $C_L$  and  $C_J$  for different values of the vortex-distance ratio ( $d' = d/R$ ) for appropriate initial vortex strengths  $\gamma_0$  determined so that  $\gamma_0/dU_\infty$  remained constant. Figures 3 and 4 show that the predicted values of  $C_L$  and  $C_J$  is strongly dependent on the vortex-distance ratio  $d'$ . The curves of both figures suggest that there are unique values of  $C_L$  and  $C_J$  when  $d' = 0$ . The curves do not continue to  $d' = 0$  because the effect that one vortex induced on its immediate neighbours became very large at small  $d'$  and the resultant motions of the sheet are best described as chaotic. To solve this problem, a vortex splitting process has been adopted, as explained below.

### 4.2 VORTEX SPLITTING

In order to study the convergence of the model's prediction, further reduction in the vortex distance is needed, without altering the contour of the vortex sheet. Reduction of the vortex distance is possible by splitting the vortices after the sheet's contour has been established. Each vortex in the sheet is divided into a group of sub-vortices. The sub-vortices are spread along the line separating this vortex from the next one. The strength of each sub-vortex is calculated in proportion with the general decay of the sheet as expressed in equation (2), provided that the total strength of a group of sub-vortices equals the strength of the original vortex which was split. This has similarities to Maskew's work (Ref.19).

The splitting process allows an indefinite reduction in the vortex distance without altering the contour of the vortex sheet, or the circulation.

Figures 5 and 6 show the results obtained by introducing the splitting process to the model. The figures show that both  $C_L$  and  $C_J$  continue to converge towards ultimate values, as suggested before by Figures 3 and 4. A wider range of investigation on different circular cylinders has concluded that if the vortex distance is eventually reduced to 0.1 per cent of the cylinder's radius, the predicted  $C_L$  and  $C_J$  values will converge to within 0.5 per cent of its ultimate values. The ultimate values are those expected if the vortex distance is reduced to zero, i.e. when the vortex sheet becomes a continuous sheet of vorticity. The model, in this form, has successfully represented a continuous sheet of vorticity by a discrete vortex model.

### 5.1 COMPARISONS WITH EXPERIMENTAL DATA

The mathematical model has been applied to a wide range of circular cylinders and its predictions compared with the corresponding experimental data. The application has covered different circular cylinder designs and flow conditions. A variety of circular cylinders have been tested and reported in Ref.(2). Two of those models have been chosen to demonstrate the vortex model's prediction capability. Figure 7 shows the comparison for a single slot model (ROMNEY MODEL 2 BUILD 4) at two angles of attack. Figure 7a represents the case when the slot was located at the top dead centre, with the wind tunnel speed at  $M_\infty = 0.2$ . In Figure 7b the slot was moved  $20^\circ$  aft from top dead centre, while the tunnel speed was at  $M_\infty = 0.34$ . The prediction has been calculated in each case for different

values of the arbitrary constant ( $K$ ), defined in the decay equation (2). The model gives an excellent prediction of the experimental results when  $K = 0.165$ . Despite the differences in free stream velocity and slot position, the same value of  $K$  has produced equally good agreement with the experiment shown in the second case (7b).

A different model (ROMNEY MODEL 2 BUILD 2) has been used for further comparison. The model employed two slots, one at top dead centre and the other at  $30^\circ$  downstream, while the wind tunnel speeds were  $M_\infty = 0.2$  and  $0.32$ , as shown in Figure (8). The discrete vortex model has been applied in this case by introducing vortices from the two slots simultaneously. Both sheets have the same intensity of vorticity, the total jet momentum coefficient is the sum of both jet momentum coefficients. The motion of each vortex is decided by the velocity induced on this vortex by all vortices in both sheets. Figure 8 shows that the prediction is consistent with that produced in the single slot model, since the value of  $K$  remains virtually unchanged. The comparison of the discrete vortex model's prediction with other circular cylinders has produced the same conclusion. The value of  $K$  remains near constant in all cases, regardless of the model's dimension, slot(s) position on free stream velocity. A similar conclusion has been obtained when the model is applied to cross-sections other than circular. An example of this application is shown below.

## 5.2 APPLICATION OF THE MODEL TO ELLIPTIC-SECTIONS

The discrete-vortex modelling may be used to represent a jet on other cross-sections. The modelling can be applied to any section provided that it can be represented by potential flow elements such as doublets, sinks, sources, etc. This representation is essential because it is used as a starting point for the discrete vortex modelling. However, an alternative method to predict the performance of a specified cross-section is to use the conformal transformation. If the required section can be produced by a suitable conformal transformation from a circular section, then the velocity distribution, as predicted from the model discussed above, can be transformed to predict the performance of the required section. This method has been used to predict the performance of an elliptic-section. The Kutta-Zhukovsky transformation has been used to calculate the velocity distribution on the elliptic boundary which allows the calculation of both lift and jet momentum coefficients of the ellipse.

A comparison with experimental results is shown in Figure 9. The experimental model is Allcock's elliptic section 10/A (Reference 3), the section has a thickness chord ratio of 20%, with the slot located at a position of  $0.874C$  from the leading edge,  $C$  being the chord of the ellipse. Figure 9 shows a similar result to that demonstrated for the circular section. A value of  $K$  within the range of  $0.15-0.165$  brings the model's prediction into very good agreement with the experimental data, further supporting the thought that  $K$  may be a constant irrespective of section.

## 6.1 BOUNDARY LAYER MODELLING BY DISCRETE-VORTICES

The previous discussion has shown that the discrete vortex modelling of the jet's shear layer successfully predicts the lift produced from an arbitrary aerofoil section with circulation control. The model in its present form cannot provide a prediction of the drag produced from such an aerofoil. An accurate prediction of the drag requires additional modelling of the surface boundary layer. The surface boundary layer is a shear layer which forms on the aerofoil boundary due to the "non-slip" condition at the surface. The surface shear layer is formed between a zero-velocity surface and an external flow of non-zero velocity, while the jet shear layer is formed between a high velocity jet flow and an external slower velocity flow. Therefore the surface shear layer can be considered as a sheet of vorticity similar to that of the jet but with the opposite sense of circulation. While the jet sheet speeds up the flow at the upper surface, the boundary layer sheet tends to slow the flow down. Therefore the circulation in the two sheets will be opposite. A discrete vortex model of the boundary layer on an unblown circular section has been developed prior to combining it with the jet model in order to predict both lift and drag.

## 6.2 UNBLOWN CIRCULAR SECTION BOUNDARY LAYER MODEL

A model of discrete vortices, which represent the boundary layer, must satisfy the boundary conditions of the flow in this layer. The velocity profile inside the boundary layer should satisfy the two basic conditions of zero velocity at the surface and a velocity at the outer edge of the profile equal to that of the potential flow. The presence of the vortices should create a velocity field which, when combined with the potential flow field, leads to a velocity profile similar to that measured in the boundary layer. Figure 10 explains how a pair of vortices (vortex + image) create a velocity profile that alters the potential flow profile into one similar to that of a boundary layer. The magnitude of the velocities in the vortex profile depend on the strength and position of the vortex relative to the circular boundary, as well as the angular distance of the vortex from the control point  $A$ .

To calculate the strength of the vortex, consider a control area as shown in Figure 11. The area lies between two arbitrary angular positions ( $\theta_1, \theta_2$ ), its internal edge is the circular cylinder surface and the outer edge lies in the flow just outside the boundary layer. The total circulation bounded by this area can be calculated as:

$$\gamma = \int q \, ds$$

where  $q$  = the velocity tangential to the area's boundary  
and  $ds$  = element of distance along the area's boundary

Since  $q = 0$  along the circle surface

$$\gamma = \int_{\theta_1}^{\theta_2} q_t \, d\theta - \int_{r_0}^{r_b} q_{n2} \, dr + 0 + \int_{r_0}^{r_b} q_{n1} \, dr$$

where  $q_t$  : Potential flow tangential velocity  
 $q_{n1}$  : Normal velocity inside the boundary layer  
 $\theta$  : Angular position measured from the leading edge

Assuming that the change in the normal velocity between positions  $\theta_1$  and  $\theta_2$  is negligible, i.e.  $q_{n1} = q_{n2}$

$$\gamma = R_0 \int_{\theta_1}^{\theta_2} q_t d\theta \quad (3)$$

The circulation calculated in this way satisfies the conditions of zero surface velocity, and that the velocity outside the boundary layer is that of the potential flow. However, if equation (3) is applied for the vortices at positions  $\theta > 90^\circ$ , the calculated circulation will decrease as  $\theta$  increases because of the reduction in  $q_t$ . This is not physically acceptable, since the boundary layer vorticity has to increase because it represents the momentum destroyed by the surface. Therefore it has been assumed that the vortex strength remains constant for the region  $\theta > 90^\circ$ . The complete modelling of the boundary layer starts by dividing the layer along the surface into (n) control areas of equal angular width. The circulation within each box is calculated according to equation (3) or according to the assumption mentioned above, then each calculated circulation is concentrated in a single vortex at the middle angular position between  $\theta_1$  and  $\theta_2$  (Fig.11). The distance of each vortex from the circular surface is decided by applying the condition of zero velocity at (n) control points on the circle. The control points are chosen at the intermediate angular positions between the vortices. These points are used as reference points for calculating the velocity profiles across the boundary layer. The application of zero velocity condition leads to (n) algebraic equations which can be solved to calculate the exact positions of the vortices. The model adopts two groups of (n) discrete vortices to represent the boundary layer at the upper and lower surfaces, but only (n) algebraic equations are solved because of the symmetry of the flow on both surfaces. The velocity profile has been calculated at each control point, and the outer edge of the profile ( $R_b$ ) is considered to be reached when the calculated velocity equals that of the potential flow.

The calculated velocity profile has been used to calculate the displacement thickness at each control point. The displacement thickness is calculated from the equations:

$$\left( \int_{R_0}^{R_d} q_t dy \right)_{PF} = \left( \int_{R_0}^{R_b} q_t dy \right)_{PF} - \left( \int_{R_0}^{R_b} q_t dy \right)_{BL} \quad \text{where } R_d = R_0 + \delta_d$$

where  $dy$ : distance element along the radial direction  
 $\delta_d$ : Displacement thickness  
 PF denotes the original potential flow  
 BL denotes the boundary layer due to vortex flow

This equation is driven from the definition of the displacement thickness as the distance by which the potential flow streamlines are displaced by the presence of the boundary layer.

The pressure coefficient at this point is then defined as

$$C_p = 1 - (q_{t,d}/U_\infty)^2$$

where  $q_{t,d}$  is the tangential potential flow velocity at the distance  $R_d$ . The pressure coefficient distribution along the surface is used to correlate the model's prediction with the experimental data. To complete modelling the flow around the circular cylinder, it is necessary to model the separated flow region behind the cylinder. The position of the separation point is decided from the calculated velocity profiles by using the definition of separation. The separation point is defined as the point where the surface shear stress vanishes, i.e. when the tangential velocity gradient at the surface becomes zero ( $\partial q_t / \partial y_s = 0$ ). This gradient has been calculated from the velocity profile at each control point until its value reaches zero. The separation is considered to occur at this position and the separation pressure coefficient is taken as the pressure coefficient of this point. Since the separated flow region has constant pressure, it is simulated by introducing a number of doublets on the surface between the separation points. The strength of these doublets are decided by applying the condition of constant separation pressure at the control points in the separated area.

The model's prediction of the pressure coefficient distribution has been compared with Achenbach's data (Reference 20) for a supercritical flow, i.e. the turbulent boundary layer is fully developed. Figure 12 shows the comparison between experiment, potential flow and model's prediction. The figure shows how the number of vortices has affected the predicted separation position and pressure. It has been found, as suggested by the figure, that the prediction converges rapidly as the number of vortices increases. If the number is increased more than 60, there is little effect on the predicted position and pressure at separation. Apart from the region between  $\theta = 85^\circ$  and  $105^\circ$ , the prediction has produced a very good agreement with the experimental data. The deficiency in the prediction in this region is probably due to the assumption of constant vorticity in the region of  $\theta > 90^\circ$ . The model's prediction is expected to improve if the vorticity increases in this region rather than remaining constant. Further investigation is required to find a formula governing the growth of vorticity in this region. The drag coefficient  $C_D$  has been calculated by integrating the predicted pressure distribution, and compared with the experimental value. The predicted pressure distribution gave a value of  $C_D = 0.768$ , while the corresponding experimental value was  $C_D = 0.755$ , that is, an error of less than 2%. The noticeable error in the model's prediction of the  $C_p$  distribution in the region of  $105^\circ > \theta > 85^\circ$  has, as expected, a very small contribution to the calculated value of  $C_D$ .

## 7. CONCLUSIONS

A theoretical model has been developed to predict the performance of an arbitrary aerofoil whose circulation is controlled by blowing. The model relies on representing the existing shear layer(s) by sheet(s) of discrete vortices rather than using the conventional boundary (shear) layer analysis. Initially, a model has been developed to predict the lift and jet momentum coefficients of a section equipped with a slot which discharges a wall jet downstream. The shear layer between the jet and the external flow has been represented by a series of vortices emerging from the slot. The model has employed a form of vortex time decay to simulate the real jet decay due to

viscous and entrainment effects. It has been assumed that the strength of decay is in proportion to the external flow momentum, the jet momentum and an arbitrary constant of decay. In comparison with experimental data, the model's prediction has shown that the value of this arbitrary constant is approximately fixed despite the wide variations in model geometry, number of slots and external flow velocity. In order to predict the drag of the circulation controlled aerofoil, a second model has been developed to represent the boundary layer on an unblown circular aerofoil, as an initial step towards combining the two models for the prediction of both lift and drag. The boundary layer, as a shear layer, has been represented in the model by a series of discrete vortices, while the separated flow region has been simulated by a group of doublets. The strength of vortices/doublets has been calculated using the boundary conditions applicable to the boundary layer and separation criteria. The model's prediction of the pressure distribution around the surface has produced reasonable agreement with the experimental data of the unblown circular section. The experimental drag coefficient is predicted theoretically, with an error of only 2%.

A combination of the jet and the unblown models is expected to result in a generalized representation which predicts both lift and drag coefficients of an arbitrary circulation controlled aerofoil. It is also expected that by combining the jet and the boundary layer sets of vortices, an explanation for the nearly constant value of decay in the jet model may be possible.

#### REFERENCES

1. I.C. Cheeseman: The lift and drag of a circular cylinder equipped for circulation control by spanwise blowing. August 1964. Unpublished NGTE Note.
2. J. Dunham: Circulation control applied to a circular cylinder. July 1967. NGTE R287.
3. A.W.R. Allcock: Observations on the lift performance of elliptical-section aerofoils with circulation control. May 1969. NGTE NT750.
4. A.R. Osborn and C.N. Sherbourne: Two-dimensional wind tunnel tests on 10 per cent and 40 per cent elliptic section models with tangential blowing slots. June 1968. NGTE PLAND Note No.5.
5. I.C. Cheeseman and A. R. Seed: The application of circulation control by blowing to helicopter rotors. July 1967. Jour. of Roy.Aer.Soc., Vol.71, No.679.
6. I.C. Cheeseman: Circulation controlled rotor aircraft. July 1969, Aircraft Engineering.
7. R.M. Williams, R.T. Leitner and E.O. Rogers: X-wing: A new concept in rotary wing VTOL. Aug. 1976, Amer.Mech.Soc. Symposium on Rotor Technology.
8. J.B. Wilkerson and D.W. Link: A model rotor performance validation for CCR technology demonstrator. 1975 31st Amer. Mech.Soc. Forum.
9. E.O. Rogers: Recent progress in performance prediction of high advance ratio circulation control rotors. 1980 6th European Rotorcraft and Powered Lift Aircraft Forum Paper No.29
10. J. Dunham: A theory of circulation control by slot blowing applied to a circular cylinder. 1968 Jnl. of Fluid Mechanics, Vol.33, Part 3.
11. G. Truaiton: Incompressible Aerodynamics, 1960, Clarendon Press, Oxford.
12. E.S. Levinsky and T.T. Yeh: Analytical and experimental investigation of circulation control by means of a turbulent Coanda wall jet. 1972 NASA CR-2114.
13. E.M. Tibbs and N. Ness: Analysis of circulation control aerofoils. 1976, AIAA Jnl. of Aircraft, Vol.13, No. 4.
14. L. Rosenhead: Formation of vortices from a surface of discontinuity. 1931, Proc.Roy.Soc. Series A, Vol.13A.
15. F.H. Abernathy and R.E. Kraussner: The formation of vortex sheets. 1961 Jnl of Fluid Mechanics, Vol.13.
16. J.H. Gerrard: Numerical computation of the magnitude and frequency of the lift on a circular cylinder. 1967 Phil.Trans.Roy.Soc., Vol.261, No.118.
17. R.V. Smith: A theoretical and experimental study of circulation control with reference to fixed-wing applications. 1976 Ph.D. Thesis, University of Southampton.
18. M.M.E. Saliman: A theoretical study of circulation controlled aerofoils and experimental application to symmetrical aerofoil. 1980 M.Sc. Thesis, University of Southampton.
19. D. Maskew: Subvortex techniques for the close approach to a discretized vortex sheet. 1977 AIAA Journal of Aircraft, Vol.14, No.2.
20. E. Achenbach: Distribution of local pressure and skin friction around a circular cylinder in cross-flow up to  $Re = 5 \times 10^6$  1968 Jnl. of Fluid Mechanics, Vol.34, Part 4.

#### ACKNOWLEDGEMENT

We gratefully acknowledge the support of Westland Helicopters Ltd. and the Procurement Executive, Ministry of Defence, for their financial support of the work reported.

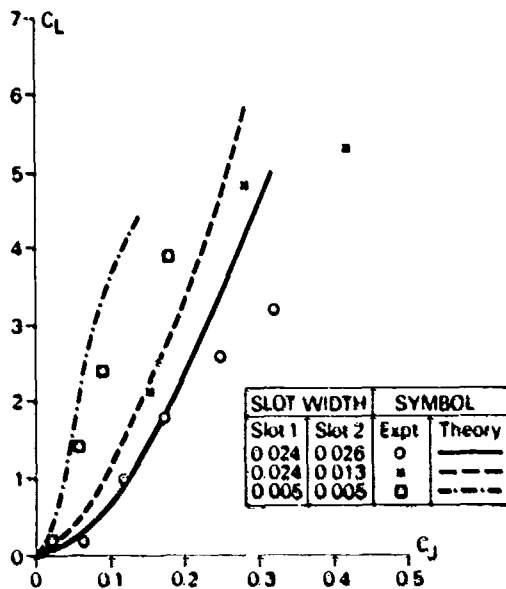


Fig. 1. Dunham's prediction of the performance of a circular cylinder with two blowing slots

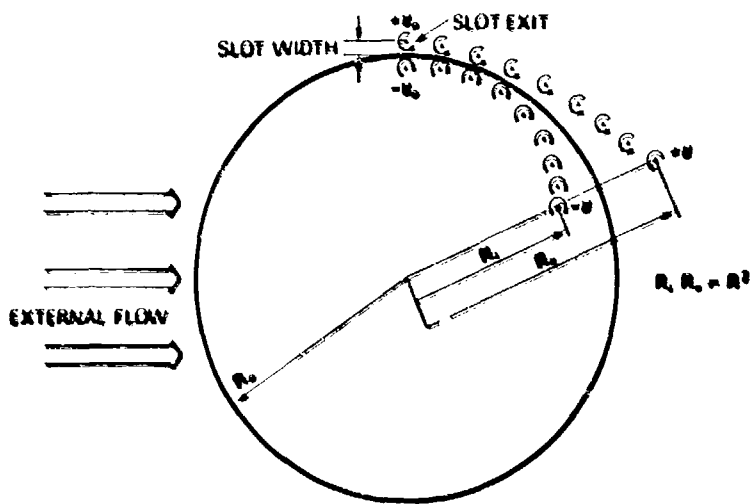


Fig. 2. Elements of potential flow model

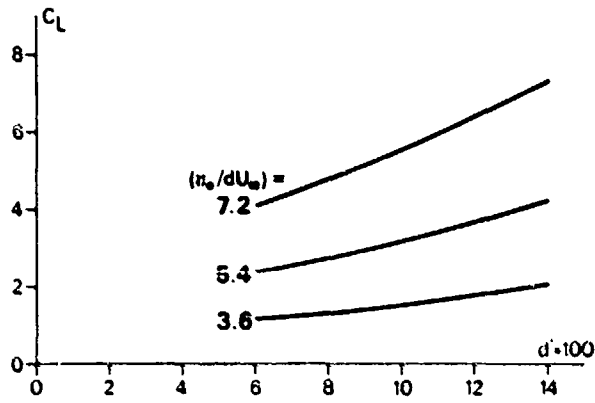


Fig.3. Influences of vortex-distance on the jet momentum predicted

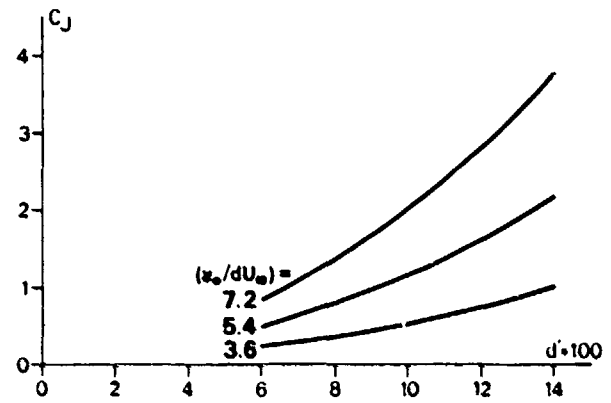


Fig.4. Influence of the vortex-distance on the lift predicted

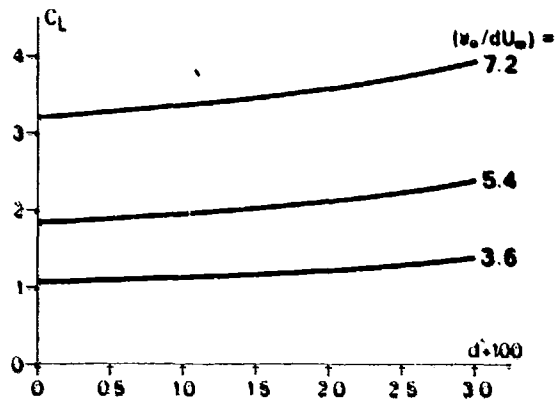


Fig.5. Convergence of lift coefficient

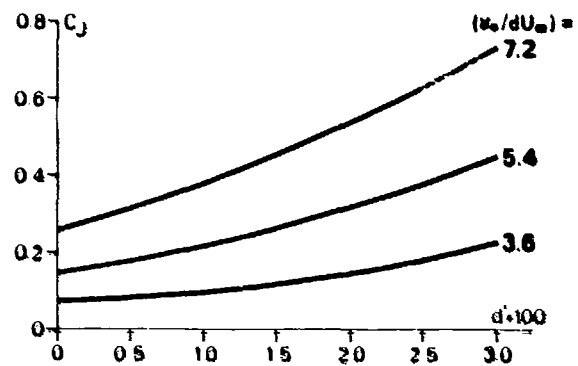


Fig.6. Convergence of jet momentum coefficient

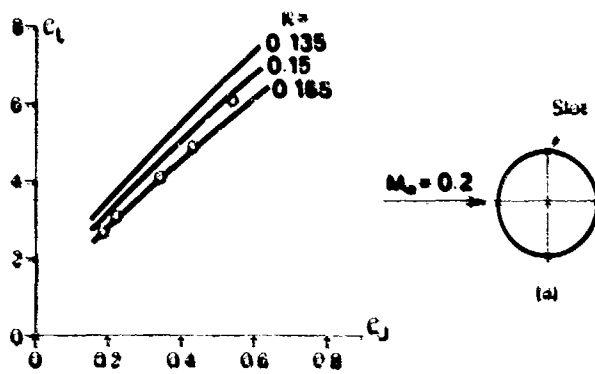
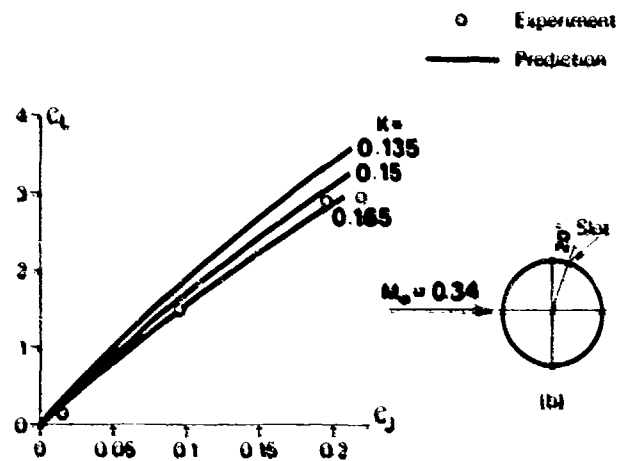


Fig.7 Runney model 2 tank 4 single slot



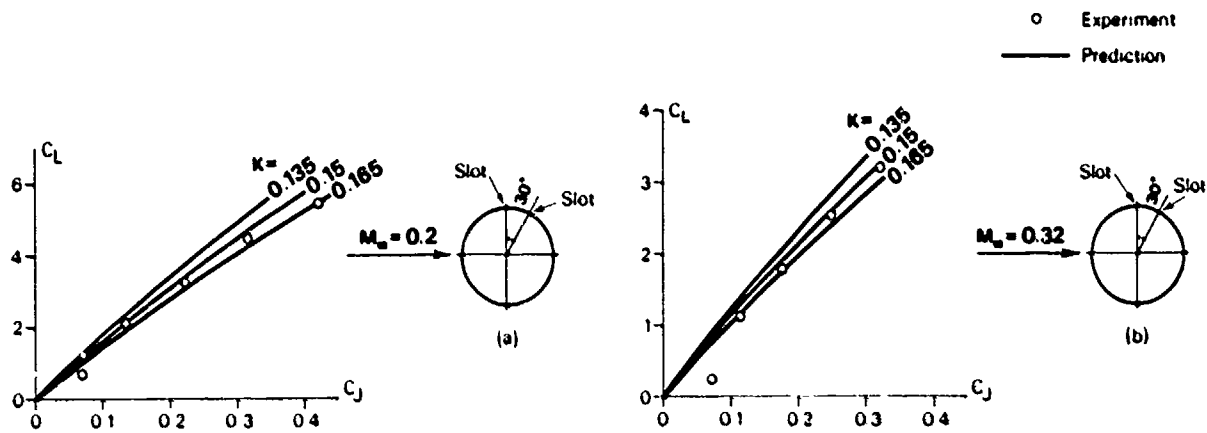


Fig. 8. Romney model 2 build 2, double slots

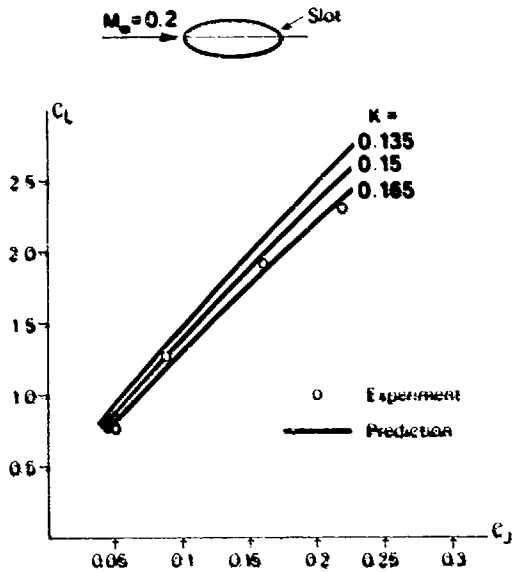


Fig. 9. Allcock ellipse model 10-A

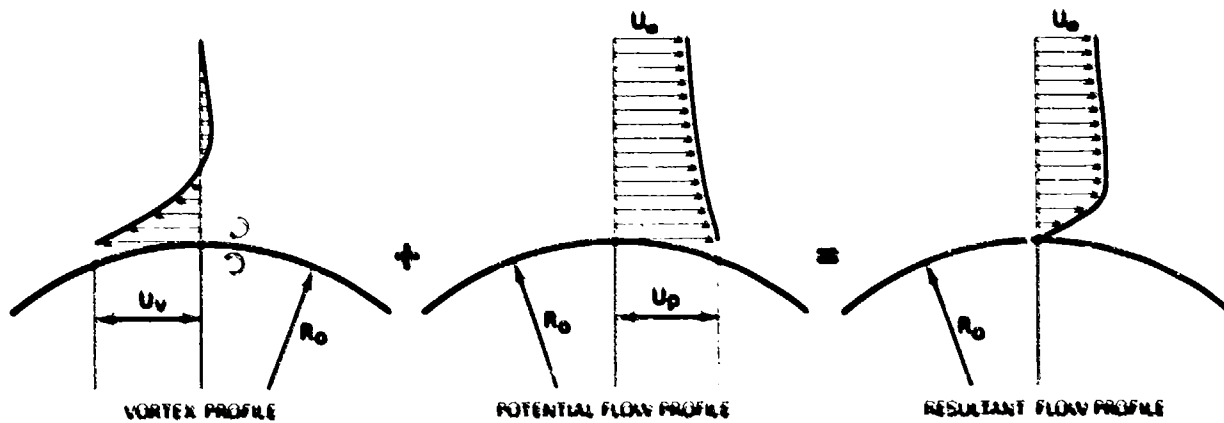


Fig. 10. Boundary layer profile formation by vortices

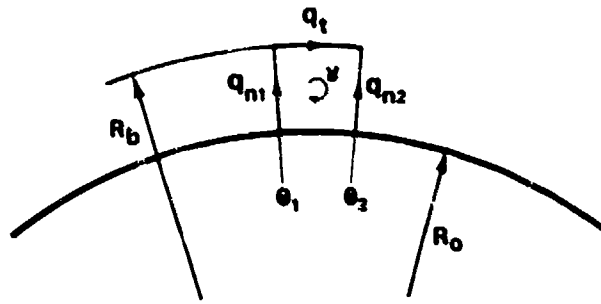


Fig 11. Vorticity inside a boundary layer element

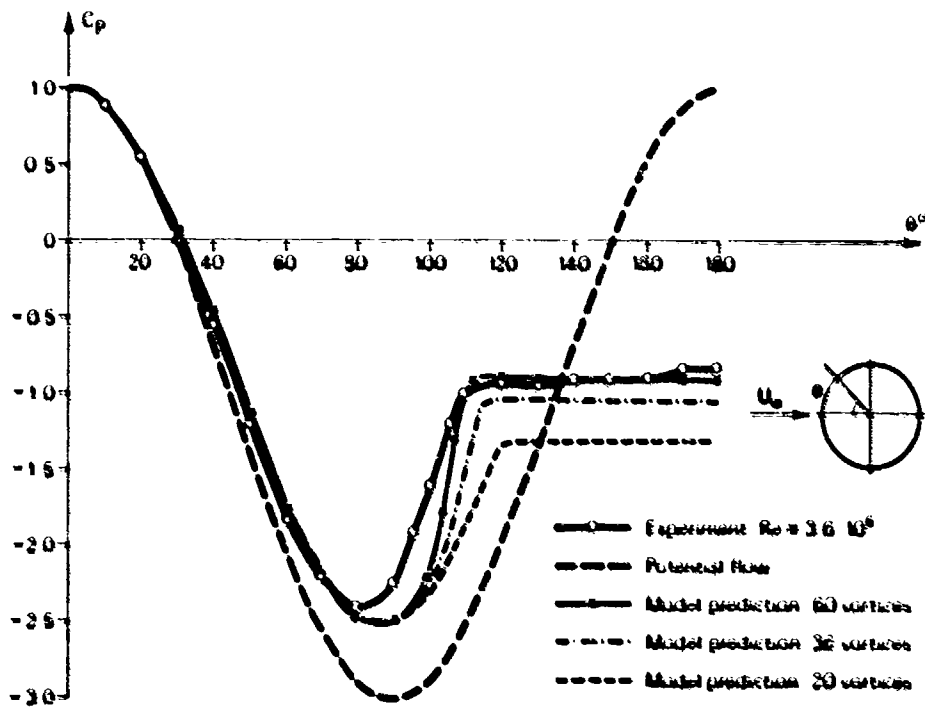


Fig 12 Pressure distributions around circular cylinder (no blowing)